SAND2019-12863C

Using the SWAT Method for Reconstructing Forces on a Drop Shock Table to Better Inform Finite Element Simulations

Brian A. Ferri
Sandia National Laboratories[1]
P.O. Box 5800 - MS0346
Albuquerque, NM, 87185

Tyler F. Schoenherr
Sandia National Laboratories[1]
P.O. Box 5800 - MS0346
Albuquerque, NM, 87185

Ryan Jennings
Kansas City National Security Campus[2]
14520 Botts Road
Kansas City, MO 64147

Abstract

Drop shock machines are commonly used to create a single sided shock pulse that is characterized by an amplitude and a pulse length. While the amplitude of the pulse input is critical in determining a majority of the stresses found in a test article, the pulse length determines the frequency content excited by the shock and can also have an effect on stress. Current simulation methods to model the drop shock machine environment typically use an experimentally measured acceleration on the surface of the drop tower carriage as the input. This measurement assumes that the surface of the drop table is rigid through the shock event, due to a lack of knowledge about the true input force

[1]Sandia National Laboratories is a multi-mission laboratory managed and operated by National Technology and Engineering Solutions of Sandia, LLC., a wholly owned subsidiary of Honeywell International, Inc., for the U.S. Department of Energy's National Nuclear Security Administration under contract DE- NA-0003525.

[2]The Department of Energy's Kansas City National Security Campus is operated and managed by Honeywell Federal Manufacturing & Technologies, LLC under contract number DE-NA0002839.

on the drop table during the shock event. The purpose of this work is to test this rigid assumption and reconstruct the input force to better characterize the shock event seen by a test article. Results from laboratory modal and drop tests, force reconstruction using SWAT, and FEM analysis are presented along with a brief background into the drop shock machine environment and the SWAT method.

Keywords
Drop Tower, SWAT, boundary condition, fixture, BARC

1 Introduction

In order to repeatedly replicate a scenario where an object falls and is met with a solid surface, such as the ground, an electromechanical shaker or drop shock machine is used in a laboratory environment. This work focuses exclusively on the drop shock machine, also referred to as a drop tower. Drop towers are especially useful in creating high G level shocks that span long time durations. However, the machines are designed such that the amplitude and the length of the pulse delivered can be changed by adjusting the height or by changing the material that the falling object contacts.

A drop tower is comprised of a few basic components starting with the table, also referred to as the carriage. The carriage is a heavy mass with a mounting surface that has tapped, threaded holes for fixturing test articles. The carriage is guided by a rail on either side that ensures that the trajectory of the falling carriage is vertical. Ideally, however, the carriage does not come into contact with the rails during the drop until the brakes are initiated upon the carriage traveling back up after bouncing at the bottom. The base of the tower is a thick and sturdy structure with an impacting surface that undergoes low displacement even during shock events. A "programmer material" is placed on the impact surface in order to prolong the deceleration of the carriage and increase the pulse length of the applied shock profile. Adjusting this lift height allows for control of the amplitude of the applied shock profile. Figure 1 displays each of the components for the Lansmont HSX30 drop tower which is located in the dynamic testing lab at the Kansas City National Security Campus. The testing and analysis performed in this work are exclusively based on this specific tower.

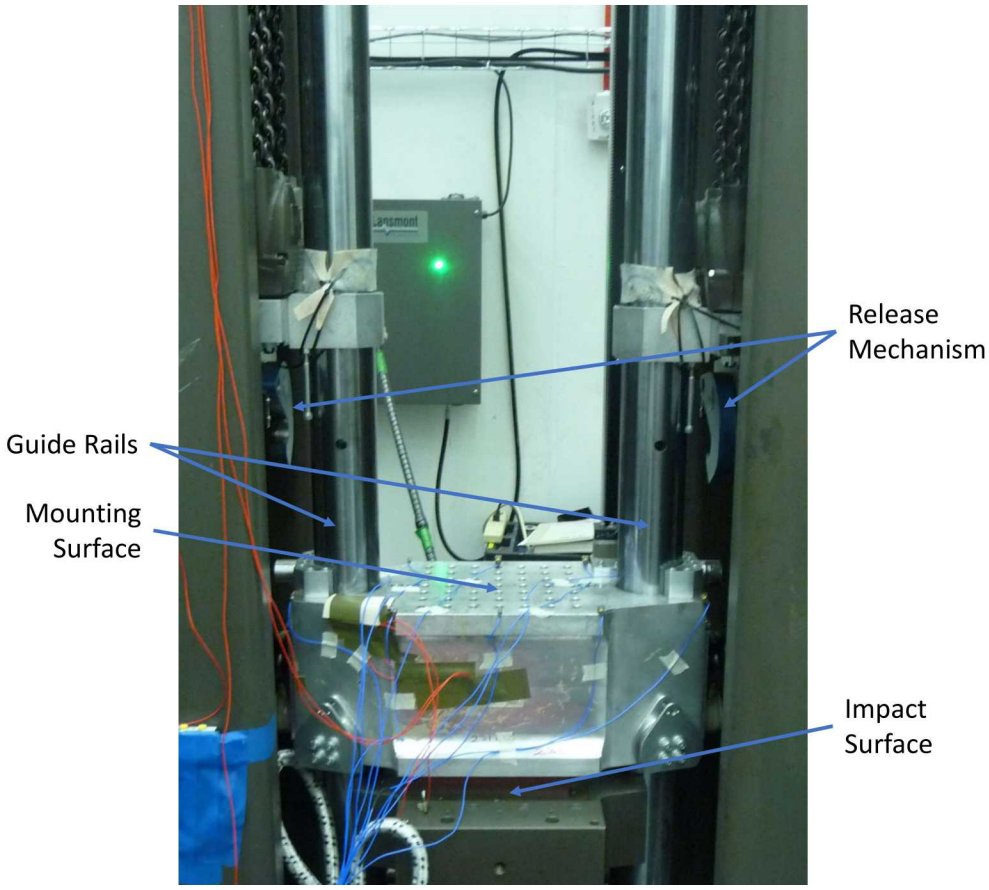

Figure 1: Drop tower components and configuration

Currently, the computational analyses of drop shock tests assume that the table, or carriage, of the drop tower is rigid through a drop event. Rigid is defined as all points within the carriage having no relative motion with respect to any other point on the carriage. To model the response of a test article, the article is fixed to a rigid surface. That surface is forced to move with the same acceleration as is measured during the test.

The rigid assumption breaks down if elastic motion of the carriage is excited during the drop environment. This dynamic response of the carriage is the primary driver for this work. In order to fully understand and characterize the drop tower, a finite element model of the carriage is developed and calibrated to the modes measured in the test performed using a modal impact hammer and 10 tri-axial accelerometers mounted at 10 locations around the top surface of the carriage.

In order to predict the carriage response in the FEM model, an input force is required. Since there is no load cell in existence that can be placed in between the carriage and the reaction mass, a experimental technique known as the Sum of Weighted Accelerations Technique (SWAT) is used. The forces calculated from the response of the carriage during drop environments are used with the calibrated model to predict drop environment response.

2 Theory

Shock testing is a standard procedure used when designing and qualifying parts and assemblies exposed to single sided pulse shocks. A drop tower converts potential energy at a given height into a haversine shaped shock pulse that reduces the momentum of the carriage and test article over a given time. The relationship between the potential energy at a specified drop height and the amplitude and duration of a haversine pulse is laid out by Deiters et al [2] and is given by Equation 1

$$\sqrt{2gh} = \frac{2A\tau}{\pi} \tag{1}$$

where A is the pulse amplitude and τ is the pulse width. From Equation 1, there is no way to adjust only the height in order to fully understand the force input. From physics however, if the impacting surface is modelled as a linear spring, then the time it takes to stop a falling object is shown by

$$\tau = \frac{\pi}{2}\sqrt{\frac{m}{k}} \tag{2}$$

where m is the mass of the carriage and test article. As the mass is constant, changing the stiffness of the programmer, k, inversely affects the change in stopping time, or pulse length. An example haversine with a 2ms pulse length and a 1G amplitude is shown in Figure 2.

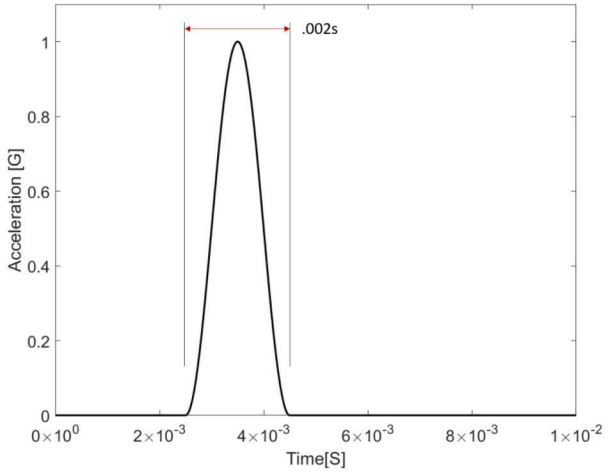

Figure 2: Half-Sine pulse with 2 a millisecond pulse length and 1G amplitude

A pulse like the one shown in Figure 2 is an ideal waveform. However, in reality, the programmer rarely behaves like a linear spring. Thus, the only way to create an analytical expression for the pulse shape is to characterize the non-linearities of the programmer through the range of motion present in the experiment. This characterization would need to be repeated for each of the programmers and quickly becomes prohibitive.

While the environments for drop shocks are described by their pulse length and amplitude, it is also important to show the frequency content of different pulses as it determines the characteristics of

the dynamic response. Figure 3 shows the same pulse as was shown in Figure 2 with 2 millisecond pulse length and 1G amplitude. A Fast Fourier Transform operation is performed in MATLAB [3] to transform the signal from the time domain to the frequency domain.

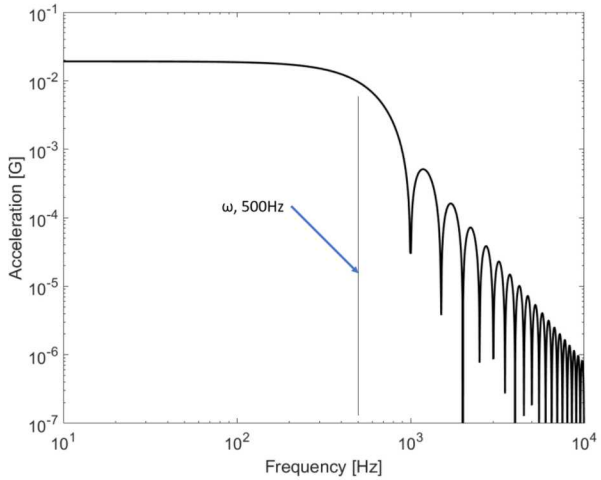

Figure 3: Fast Fourier Transform of haversine impulse

As shown in the figure, the frequencies up to 500Hz or $1/\tau$ are all equally present in magnitude in the haversine pulse. After 500Hz, the magnitude of the frequency decays exponentially (or linearly on a log-log plot such as the one in Figure 3). Thus, as the the pulse length of the impulse decreases, the range of equally present frequency content that exists will increase to a broadband limit.

Another way that shock profiles are commonly characterized in the mechanical environments community is by their shock response spectrum (SRS) shown in Figure 4.

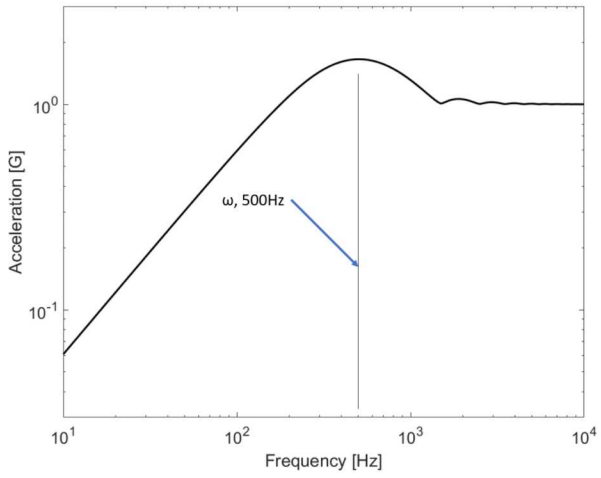

Figure 4: Shock Response Spectrum of haversine impulse

In order to develop a model of the drop tower environment, an accurate depiction of the input

load is needed. The SWAT and SWAT-TEEM algorithms are used as methods to determine the input to the drop tower environment. These algorithms have been used in previous works [1] [4] [5] to calculate external forces acting on the unit of interest in various environments and detailed derivations for both algorithms can be found in the work by Schoenherr [6].

The expressions for SWAT is reproduced here as

$$[M_r\ 0]\boldsymbol{\phi}^{+}\ddot{\bar{x}} = \boldsymbol{\phi}_r^T \bar{F} \tag{3}$$

and SWAT-TEEM as

$$\left[M_r\ 0\right] \cdot \left[\boldsymbol{\phi}_r\ \ddot{\bar{x}}_{fd}\right] \ddot{\bar{x}} = \boldsymbol{\phi}_r^T \bar{F}, \tag{4}$$

where M_r are the masses and inertias of the test unit, $\ddot{x}_{fd}$ are the accelerations of the test unit undergoing free decay, $\boldsymbol{\phi}$ is the matrix of mode shapes of the test unit with the subscript r designating rigid body modes, the superscript $^{+}$ is the Moore-Penrose psudoinverse, $\ddot{\bar{x}}$ are the accelerations of the test unit during the environment, and $\bar{F}$ is the external forces acting on the test unit.

Equations 3 and 4 deserve more explanation with respect to their similarities and differences. Both techniques solve for the sum of all the external forces resolved at the test unit's center of gravity designated as $\boldsymbol{\phi}_r^T \bar{F}$. Both techniques also solve for a weighting vector that is premultiplied by the time domain responses of the test unit. The difference between the two techniques is the weighting vector. The SWAT algorithm uses the mode shapes of the test unit to eliminate the elastic motion from the measured accelerations whereas the SWAT-TEEM algorithm uses the measured accelerations of the test unit after all of the external forces are zero.

For SWAT-TEEM to be applicable, the test unit must experience a period of time where no external forces are acting on it. It is only during this time where the $\ddot{\bar{x}}_{fd}$ can be extracted from the full measured set of data, $\ddot{\bar{x}}$. The benefit of this method over SWAT is that a set of mode shapes do not have to be measured and slight differences in configuration do not degrade the result because the filter is computed based on the configuration used during the actual environment.

3 Modal Analysis

3.1 Analytical Modal Analysis

A model of the carriage is constructed and is displayed in Figure 5.

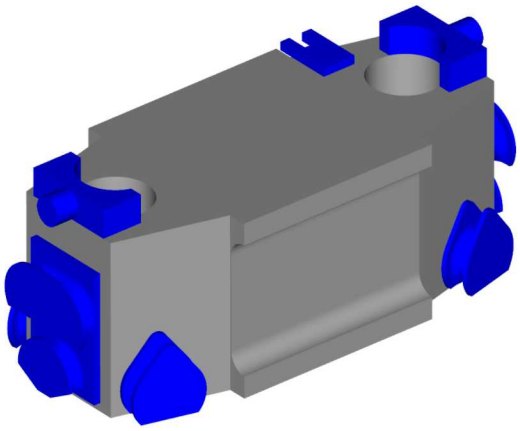

Figure 5: Full model of drop tower carriage with all mechanical hardware attached

The modes for the system were found using Sierra SD [9] on a model that included the carriage plus some of the mechanical hardware. The Sierra SD model is comprised of roughly 400,000 ten node tetrahedral elements. All of the component surfaces are tied together and the bolted joints are not modeled. The primary material is Aluminum 7075 which makes up the carriage and a few of the hardware components. A mesh refinement study is performed and converges with respect to the natural frequencies calculated. The mass of the model is 229.5 lbs compared to 233 lbs measured in the lab.

The model is calibrated to an experimental modal analysis test described in Section 3.2, and Figures 6 through 8 show the modes of the carriage.

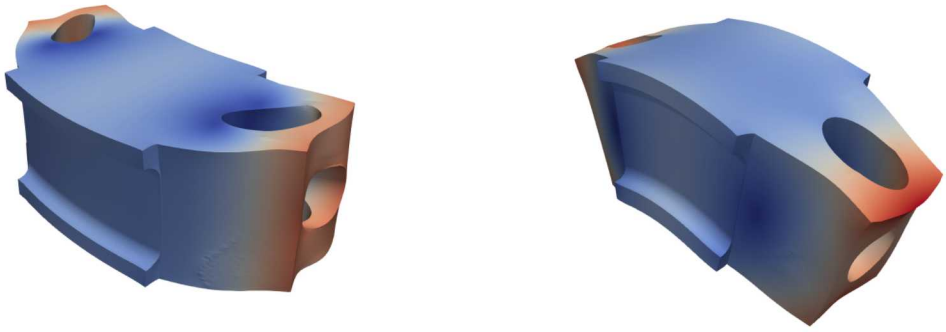

(a) 1st elastic mode
2177 Hz

(b) 2nd elastic mode
2258 Hz

Figure 6: First two elastic modes of the drop tower carriage found with Sierra SD

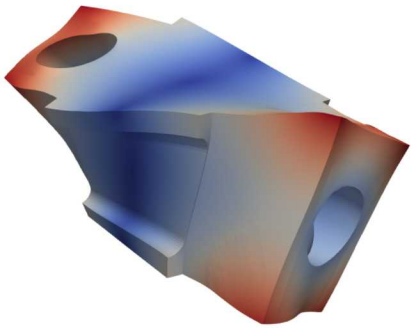

(a) 3rd elastic mode
2291 Hz

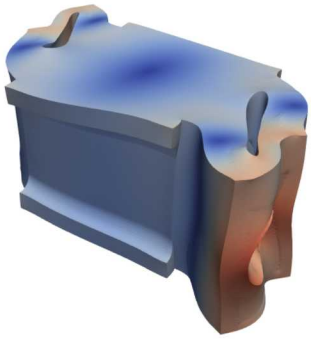

(b) 4th elastic mode
3372 Hz

Figure 7: 3rd and 4th elastic modes of the drop tower carriage found with Sierra SD

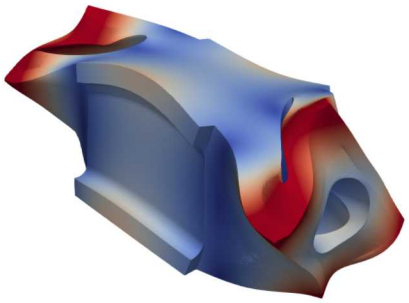

(a) 5th elastic mode
3396 Hz

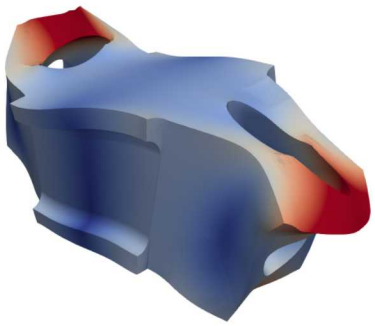

(b) 6th elastic mode
3531 Hz

Figure 8: 5th and 6th elastic modes of the drop tower carriage found with Sierra SD

3.2 Experimental Modal Analysis

An experimental modal analysis was performed to validate the results of the analytical modal analysis. The test was performed on the drop shock machine carriage, in a replicated free-free condition by placing foam underneath the carriage and letting the carriage rest on the foam. Ten tri-axial accelerometers were used to measure the response on the top surface of the carriage. The experimental setup can be seen in Figure 9.

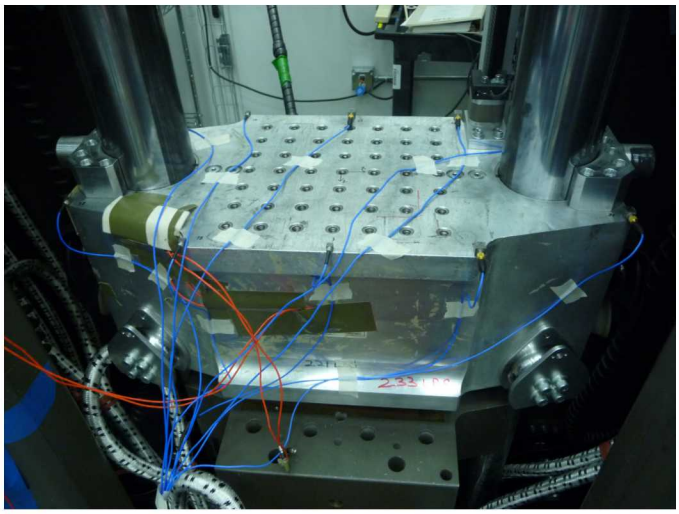

Figure 9: Experimental Modal Analysis Setup

A modal impact hammer was used to impact the carriage in various locations, and the hammer and accelerometer responses were captured with a data acquisition system. LMS software [7] was used to determine the mode shapes and frequencies for five of the first six elastic modes. The test setup was not successful in capturing the fourth elastic mode, but that was acceptable because the main concern was capturing the modes with motion in the direction of travel of the carriage.

The mode shapes and frequencies were then compared to the analytical modes of the calibrated model. The comparisons can be seen in Figure 10 through 12.

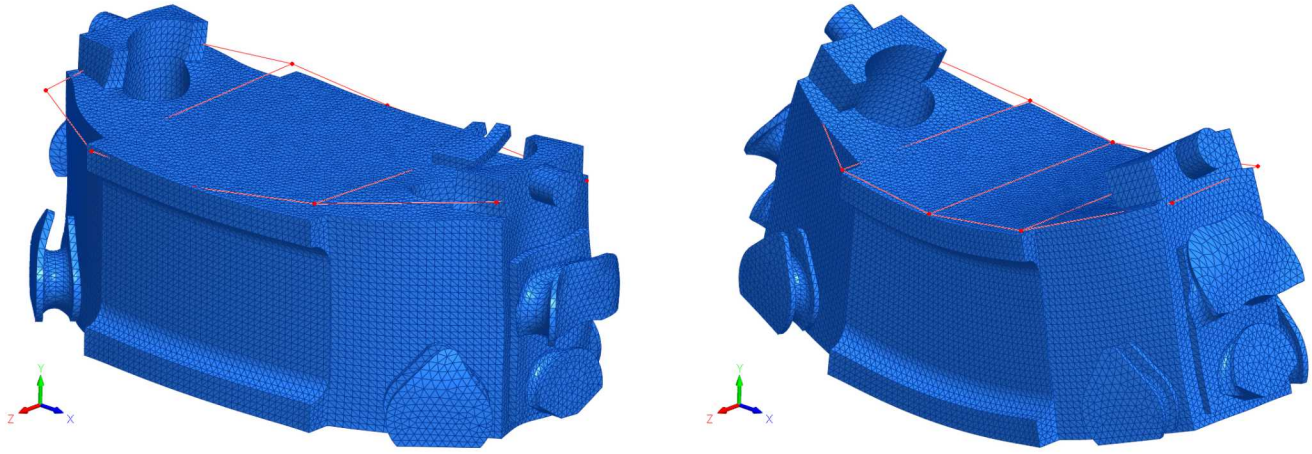

(a) 1st elastic mode
Analytical: 2177 Hz
Experimental: 2202 Hz

(b) 2nd elastic mode
Analytical: 2258 Hz
Experimental: 2257 Hz

Figure 10: Comparison of first two elastic modes found experimentally vs analytically

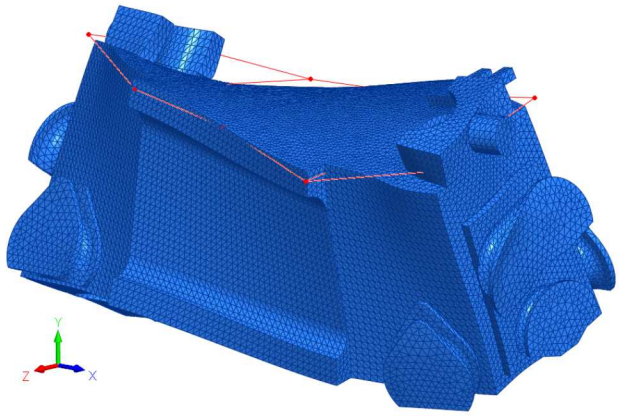

(a) 3rd elastic mode
Analytical: 2291 Hz
Experimental: 2458 Hz

(b) 4th elastic mode not found experimentally

Figure 11: Comparison of the third elastic mode found experimentally vs analytically

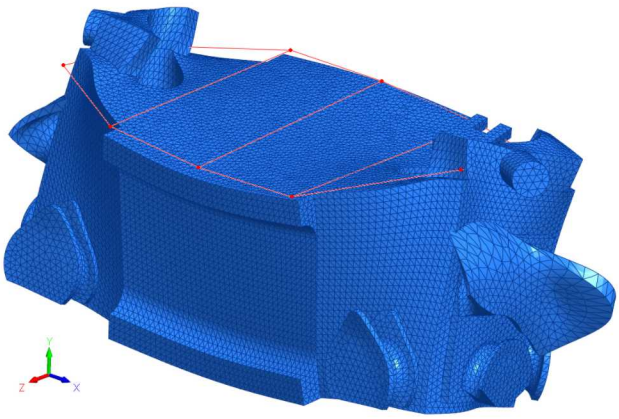

(a) 5th elastic mode
Analytical: 3396 Hz
Experimental: 3296 Hz

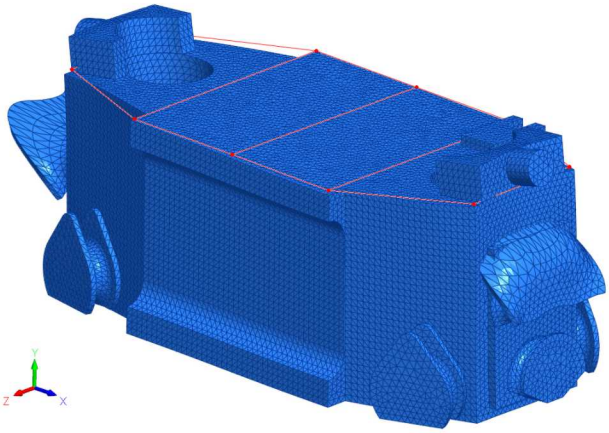

(b) 6th elastic mode
Analytical: 3531 Hz
Experimental: 3584 Hz

Figure 12: Comparison of the fifth and sixth elastic modes found experimentally vs analytically

The modal assurance criterion (MAC) plot computed using FEM Tools [8] is shown in Figure 13. The experimental analytical mode shape and frequency match very well for the second elastic mode, and reasonably well for the first, third, fifth, and sixth elastic modes. Pretest predictions showed that the 2nd elastic mode was the most important mode with respect to the SWAT technique.

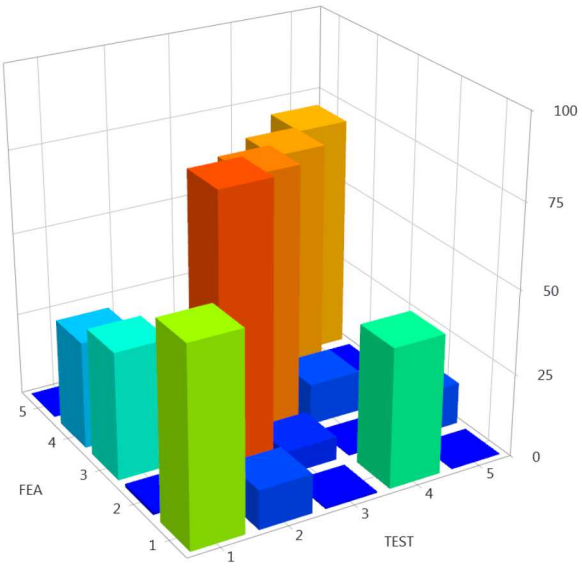

MAC values

1st elastic mode: 59%

2nd elastic mode: 87%

3rd elastic mode: 79%

5th elastic mode: 74%

6th elastic mode: 71%

Figure 13: MAC plot of 1st, 2nd, 3rd, 5th, and 6th elastic mode shapes found experimentally vs analytically

4 Drop Tower Force Reconstruction

4.1 Experimental Drop Shock Environment

After the conclusion of the modal tests, the carriage is dropped from many different heights onto many different programmer materials. The programmer materials include different size and quantities of felt sheets, and gaskets, as well as differently sized and shaped polymeric programmers. Ten tri-axial accelerometers are used to measure the response on the top surface of the carriage in the same locations as the modal tests. The experimental setup is shown in Figure 14.

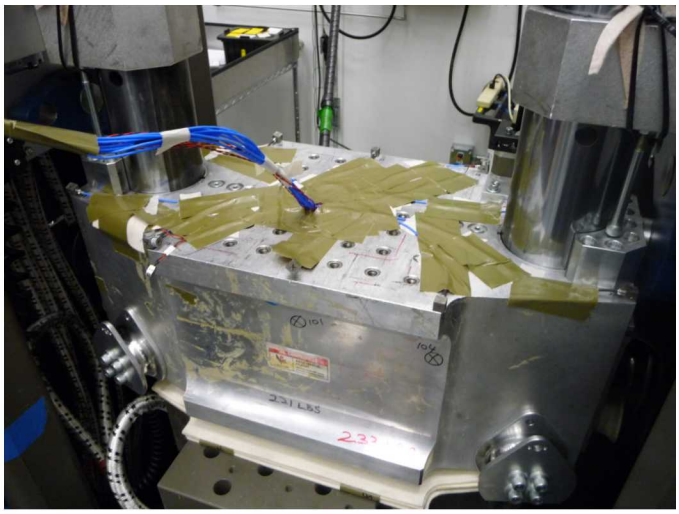

Figure 14: Experimental setup for drop shock tests

The force on the carriage is calculated for three of the experimental drops with varying pulse widths. The lift and release mechanism for the HSX30 has a sensor that records the drop height to a 0.5" precision. Parameters for the three drop tests can be seen in Table 1.

Table 1: Drop test parameters for tests on which forces are reconstructed

Run #	Drop Height (in)	Pulse Width (ms)	Max Accel (g)
004	34	1.0	1400
021	12	0.3	2000
025	5	0.1	2500

For the purposes of illustrating the SWAT method in this paper, runs 04, 21, and 25 are shown as examples. Run 04 used a single 1/4 inch piece of felt and two 1/16 inch pieces of felt as programmer. Run 21 used a single 1/8 inch piece of gasket as programmer. Run 25 used a single 1/32 inch piece of gasket as programmer. These programmer materials can be seen in Figures 15 through 17 .

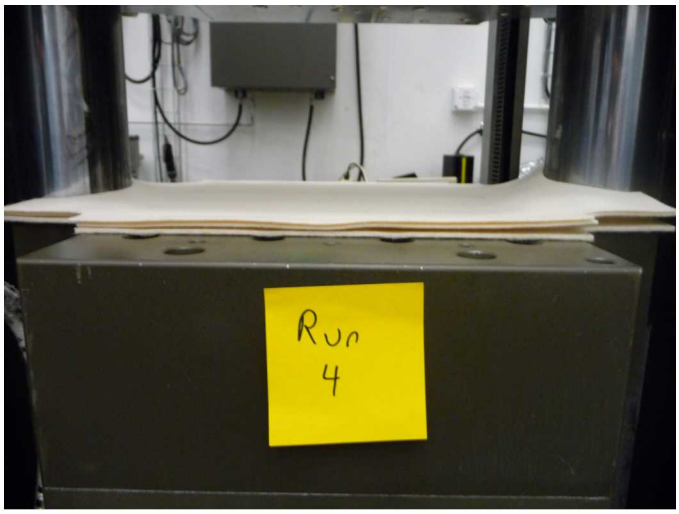

Figure 15: Programming material used in run 04

Figure 16: Programming material used in run 21

Figure 17: Programming material used in run 25

By varying the combination of programming material and drop height in a drop shock test, different pulse lengths and amplitudes for the shock are achieved. The accelerometer responses for those runs are shown in Figures 18 through 20. Each run shows that each measurement has a different representation of the impulse as the elastic motion of the carriage affects the response on the top surface of the carriage. The differences increase along with the oscillations the shorter the time duration on the impulse.

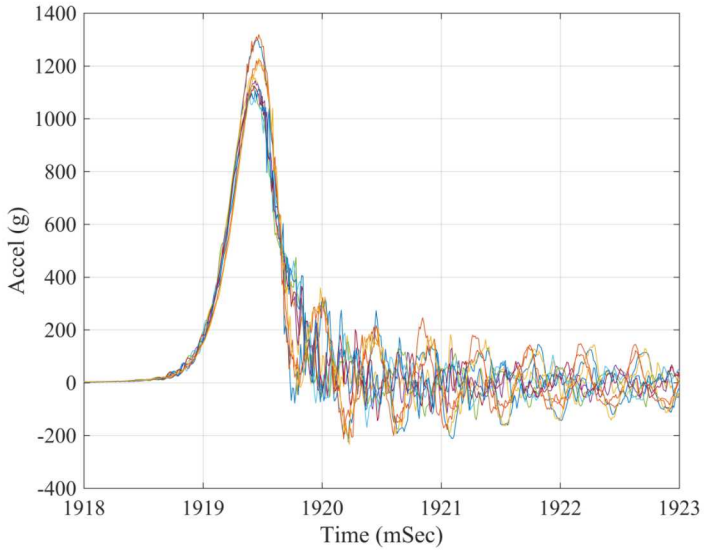

Figure 18: Accelerometer responses during run 04

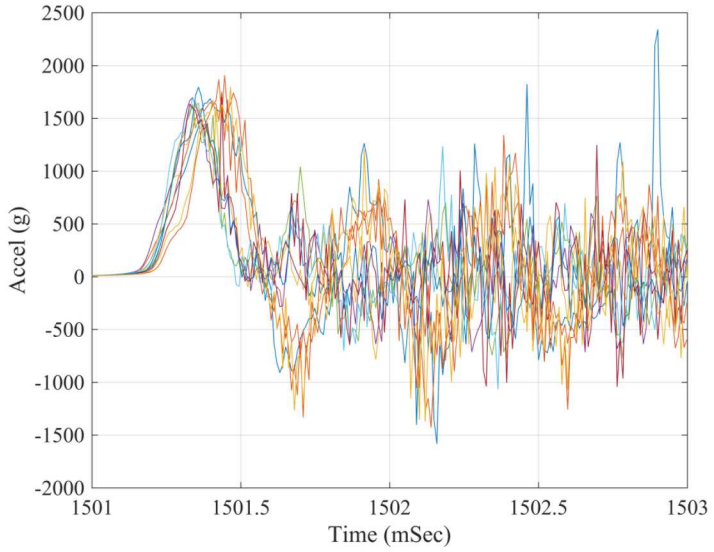

Figure 19: Accelerometer responses during run 21

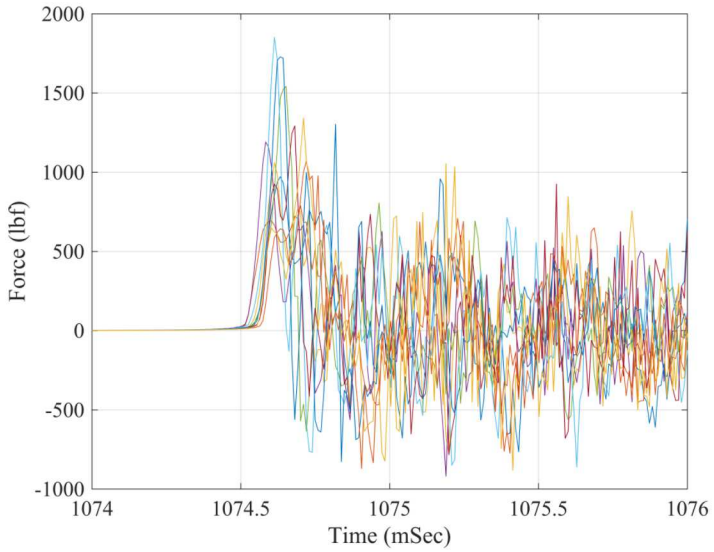

Figure 20: Accelerometer responses during run 25

4.2 SWAT Analysis

The force from the three drops are reconstructed using the SWAT and SWAT-TEEM algorithms. The SWAT algorithm uses the 1st and 2nd bending modes fit from the experimental modal analysis test. In order to compare the reconstructed forces to current force methods, the response from the accelerometer that is closest to the center of the carriage is scaled with the mass to provide a force. This scaled accelerometer force is the same as $F = ma$ where F is the force, m is the system mass, and a is the system acceleration. This force is correct if there is no elastic motion in the carriage and is represented in Figures 21 through 23 and is designated as "Scaled Accel". All of the forces

compared are low-pass filtered with a cutoff frequency of 7kHz.

Run 04, shown in Figure 21, has the longest impact pulse width of the three examples. The longer pulse width means lower frequency force is input to the carriage. Even though the first natural frequency of the carriage is excited and is measured by the response, most of the pulse is constructed of lower frequency energy. The scaled measured acceleration only has 5% error with respect to its peak value and about an error of 0.2ms with respect to the pulse length due to the carriage having only a little elastic motion.

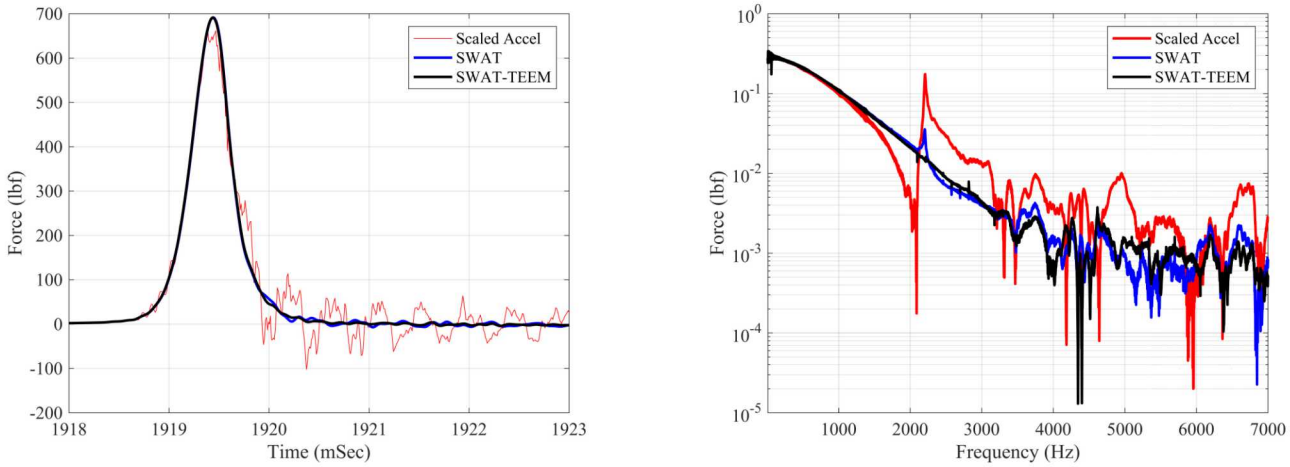

(a) Time Domain

(b) Frequency Domain

Figure 21: Forces calculated from run04

Run 21, shown in Figure 22, has a shorter input pulse width that excited the first natural frequency of the carriage enough to distort the input pulse. The dynamics measured by the accelerometer make the pulse appear to be a shorter duration and approximately 10% higher amplitude. There is also significant "input" after the pulse which is the motion of the carriage in resonance. The amplitude of the response is dependent on where the motion is measured.

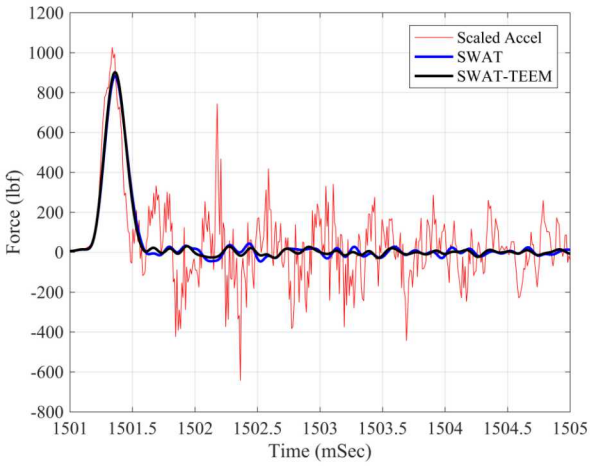

(a) Time Domain

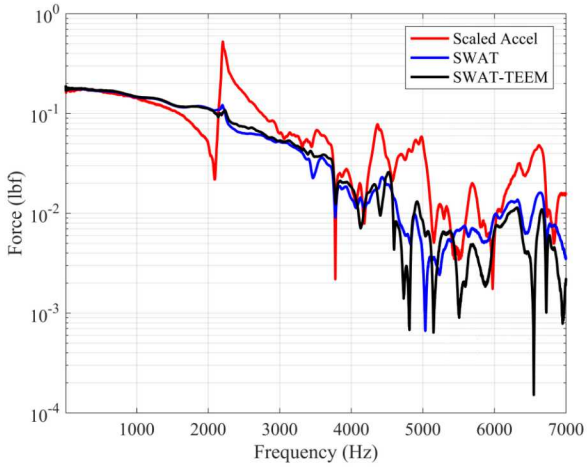

(b) Frequency Domain

Figure 22: Forces calculated from run21

Run 25 has the shortest pulse duration input that excites the dynamics of the carriage to levels comparable to the input pulse as the scaled acceleration input is calculated to be about two times the amplitude and half the width of the actual pulse. This input is also dependent on the measured location. The scaled accelerations from the different locations provide very different input definitions with respect to each other and the reconstructed force in Figure 23. For this environment, the 7 kHz filter was applied to both the scaled accelerometer pseudo force and the SWAT forces. The true force has frequency content above 7 kHz. This means that the input is only valid for frequencies less than 7 kHz when examining the system response. In this case, if the failure mode is above 7 kHz, then an alternate method should be used.

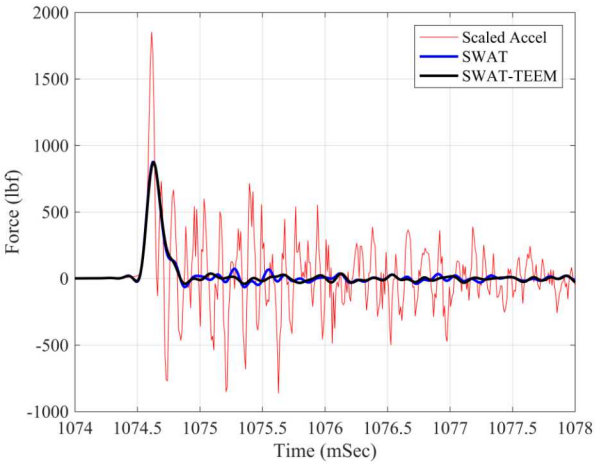

(a) Time Domain

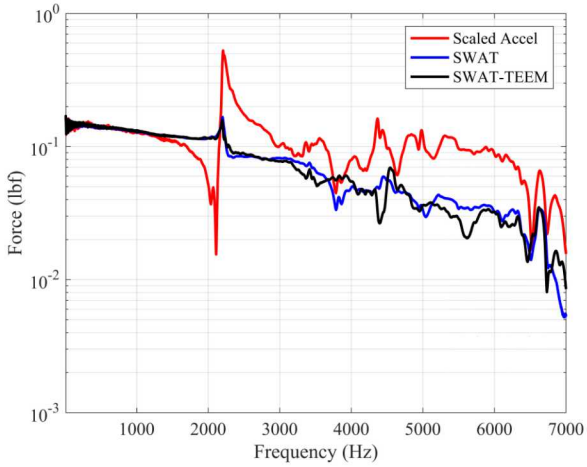

(b) Frequency Domain

Figure 23: Forces calculated from run25

5 Force and Model Validation

In order to show how the Sierra SD model compares to the experiment, the SWAT input from run21 is used as a pressure input in a Sierra SD simulation. An area of faces on the model that corresponds to the programming material is chosen and a pressure load that is proportional to the SWAT force magnitude is applied in the Y direction over the entire area. The model damping is 3% and the first bending mode in Y has an additional 1% damping applied in a modal transient analysis. Figure 24 shows the model setup.

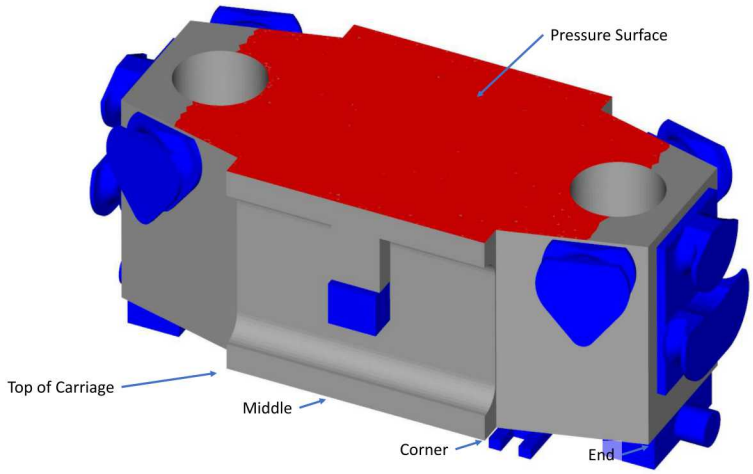

Figure 24: Sierra SD model setup for force validation

All of the measured locations are analyzed, but for this paper, the end, corner, and middle locations of interest (shown in Figure 24) are displayed. The time and frequency response for these locations in the Y direction are shown in Figures 25 through 27.

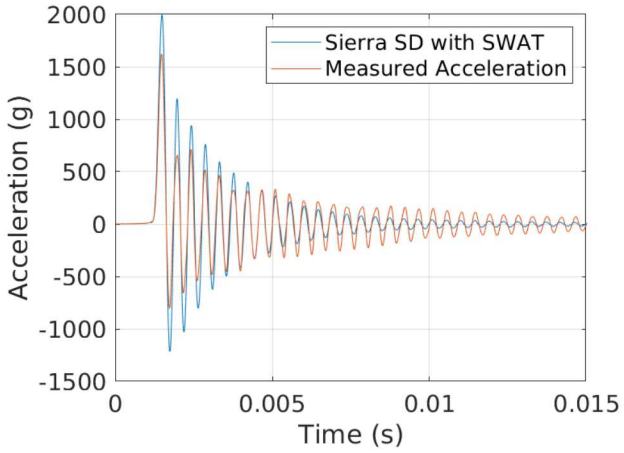

(a) Time Response

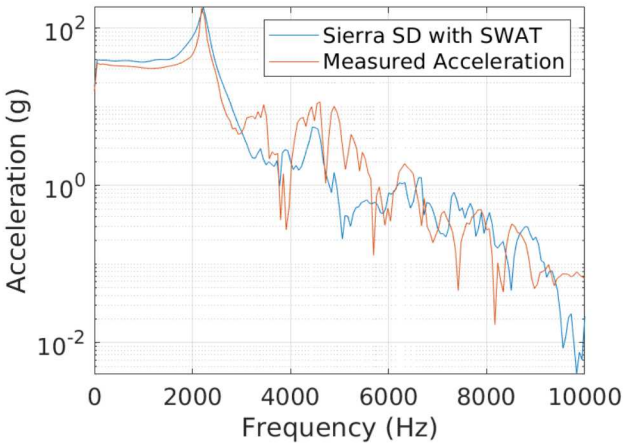

(b) FFT of Time Response

Figure 25: End response from Sierra SD with SWAT input compared to measured in the Y direction

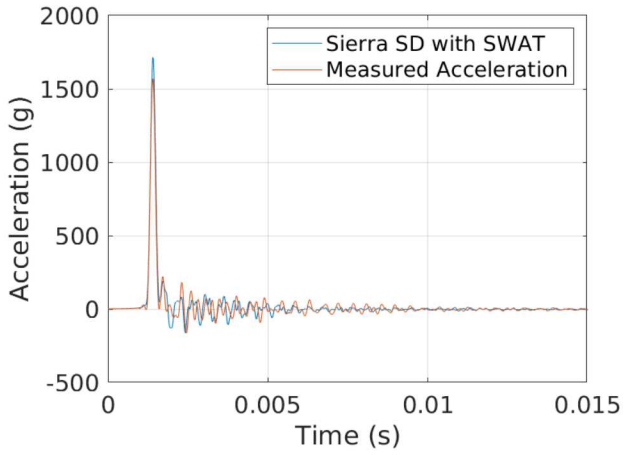

(a) Time Response

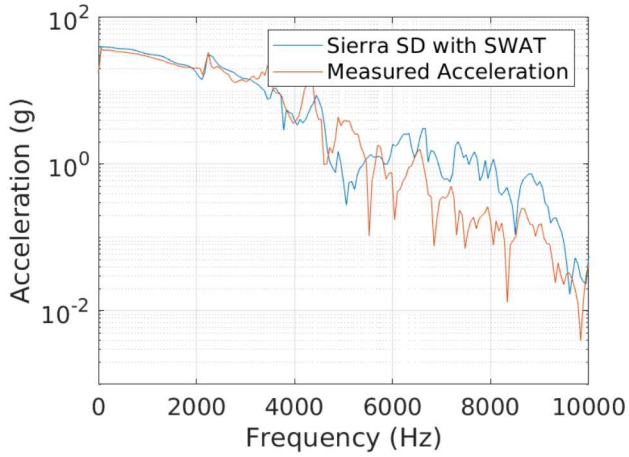

(b) FFT of Time Response

Figure 26: Corner response from Sierra SD with SWAT input compared to measured in the Y direction

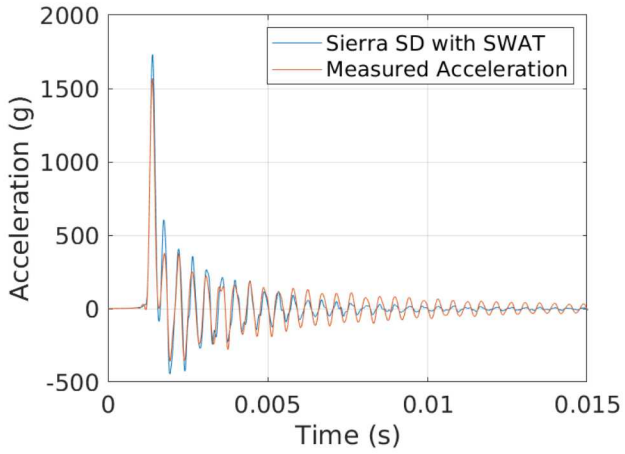

(a) Time Response

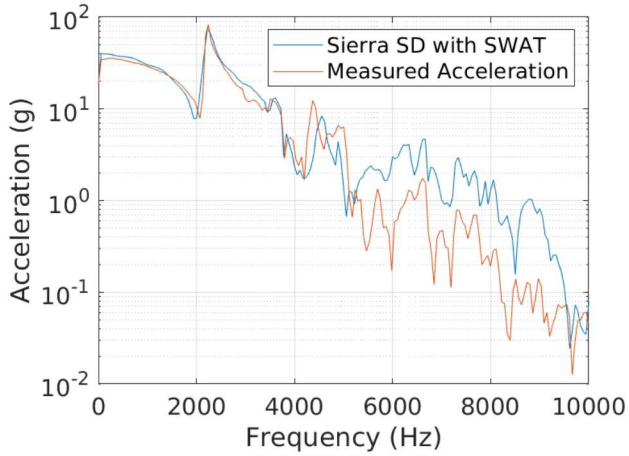

(b) FFT of Time Response

Figure 27: Middle response from Sierra SD with SWAT input compared to measured in the Y direction

As seen in Figures 25 through 27, the magnitude of the initial pulse increases from the end to the middle and the FFT of the signal shows more distinct response from the mode at 2258 Hz corresponding to the first bending mode in the Y direction.

In addition to the good agreement in the Y direction at all of the measured locations, Figures 28 and 29 show how the model also agrees with the measured X acceleration at the end and the measured Z acceleration respectively.

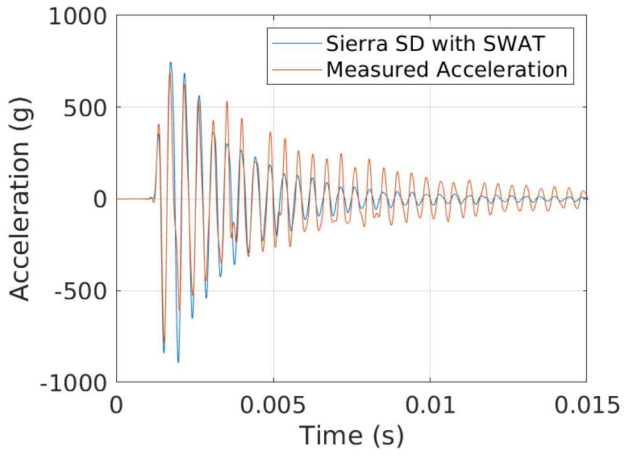

(a) Time Response

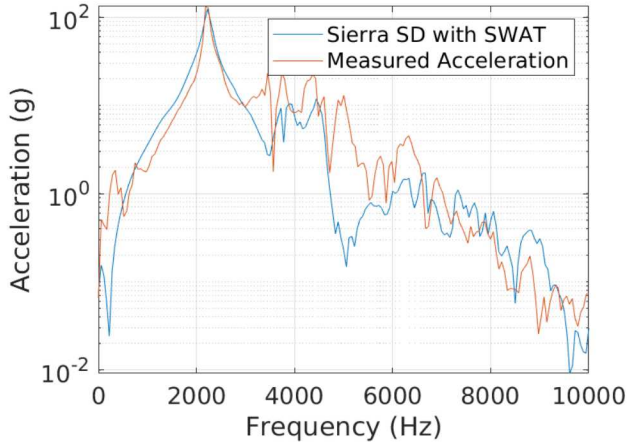

(b) FFT of Time Response

Figure 28: End response from Sierra SD with SWAT input compared to measured in the X direction

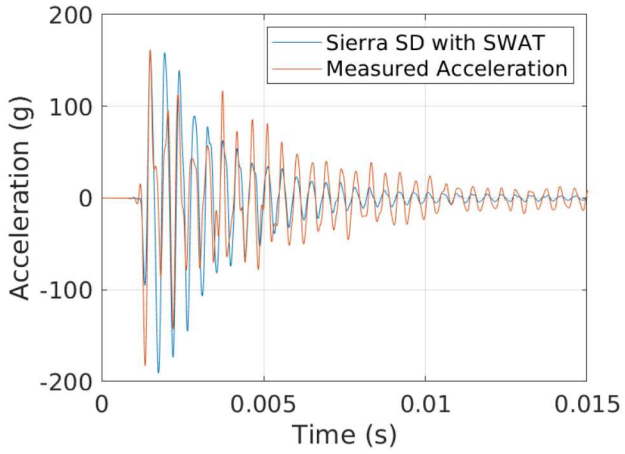

(a) Time Response

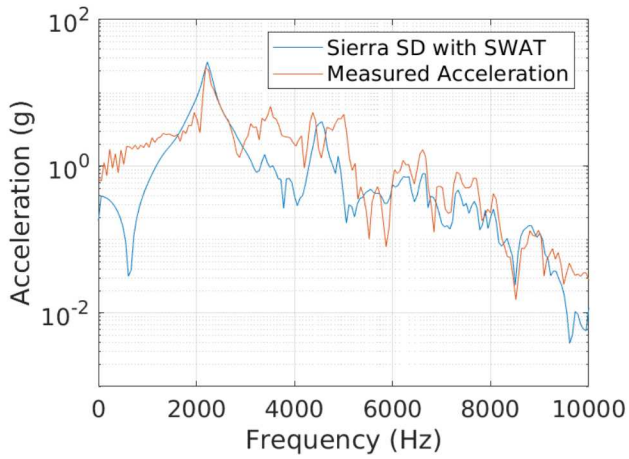

(b) FFT of Time Response

Figure 29: Middle response from Sierra SD with SWAT input compared to measured in the Z direction

The response that showed the greatest discrepancy between Sierra SD and the test was the X direction response at the middle of the carriage shown in Figure 30.

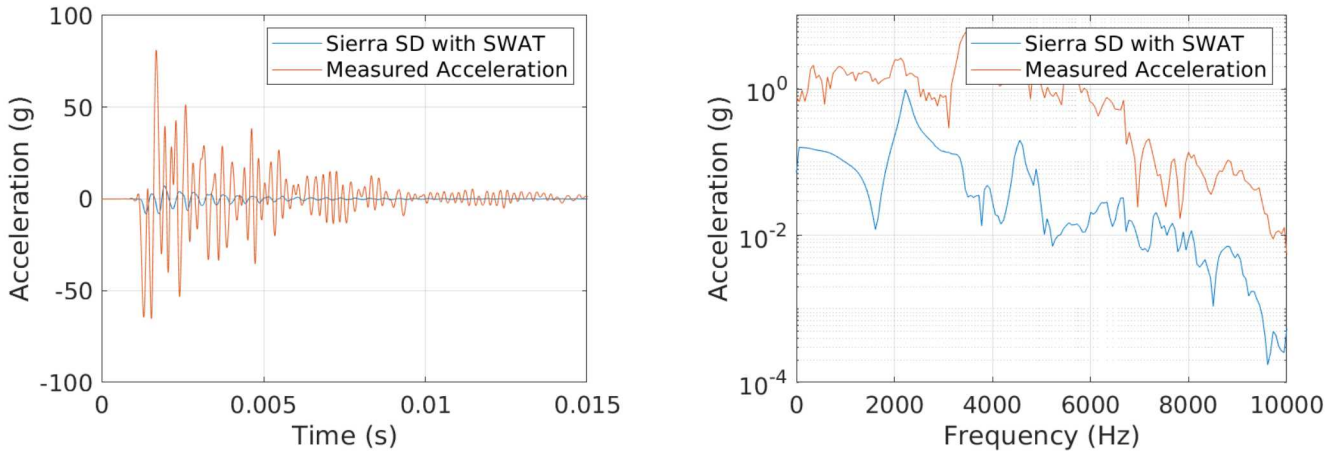

(a) Time Response

(b) FFT of Time Response

Figure 30: Middle response from Sierra SD with SWAT input compared to measured in the X direction

Figure 30 shows that there were secondary impacts which were most likely metal on metal to induce the high frequency response.

The comparison of the response between the model and the experiment is a concatenation of all of the errors within the process. These errors include model form error, the inability to characterize any intermittent impact or rattling forces acting on the carriage, or errors in SWAT. With respect to the error in SWAT, the error in this case study would be realized as the force showing an oscillating at a specific frequency due to the SWAT theory.

6 Conclusion

This work shows how the dynamics of the carriage of a drop shock machine can affect the measured response depending on choices made in instrumentation. Given a single accelerometer on the carriage, an analysis using the measured acceleration as an input to a simulation could give an incomplete response and would disclude the base strain being imparted on the unit under test.

The SWAT technique is able to use the carriage measured response to create a force input. The calculated force input is validated by applying it to a calibrated model as the model showed good agreement to the measured accelerations.

References

[1] T.G Carne, V.I. Bateman, and C.R. Dohrmann. Force reconstruction using the inverse of the mode-shape matrix. Technical Report SAND90–2737, Sandia National Laboratories, 1990.

[2] Thomas A. Deiters Mary Baker Kyle C. Indermuehle and Charles W. Engelhardt. Using analysis to design for drop or other shock environments. *Sound and Vibration*, October 2000.

[3] Mathworks. Matlab r2019a, 2019.

[4] Randy L. Mayes. Measurement of lateral launch lads on re-entry vehicles using swat, proceedings of the 12^{th} International Modal Analysis Conference. pages 1063–1068, Feburary 1994.

[5] Tyler F. Schoenherr. Reconstructing forces from continuous connections using swat. In James De Clerck, editor, *Topics in Modal Analysis I, Volume 7*, pages 65–75. Springer International Publishing, 2014.

[6] Tyler F. Schoenherr. Calculating the impact force of supersonic hail stones using swat-teem. In Alfred Wicks, editor, *Shock & Vibration, Aircraft/Aerospace, and Energy Harvesting, Volume 9*, pages 67–79. Springer International Publishing, 2015.

[7] Siemens. Testlab 17, 2019.

[8] Dynamic Design Solutions. Femtools 4.0.1, 2017.

[9] Sierra Structural Dynamics Development Team. Sierra structural dynamics - user's notes. Technical Report SAND2017-3553, Sandia National Laboratories, April 2017.